**Proceedings of the 15th International Symposium on the Packaging and Transportation of Radioactive Materials**
**PATRAM 2007**
**October 21-26, 2007, Miami, Florida, USA**

# CFD SIMULATIONS OF FUEL CLADDING AND BASKET SURFACE TEMPERATURES IN AN MPC RAIL CASK DURING NORMAL TRANSPORT

**Mithun Gudipati, Research Assistant**
**University of Nevada, Reno**
**Reno, NV 89557**

**Miles Greiner, Prof. of Mech. Engineering**
**University of Nevada, Reno**
**Reno, NV 89557**
**greiner@unr.edu, (775) 784-4873**

## ABSTRACT

A two-dimensional finite volume model of a 21 PWR Multi-Purpose Canister (MPC) inside a rail cask was constructed. In that cask, fuel is loaded into a basket structure inside an MPC. The MPC is sealed, filled with a non-oxidizing cover gas, and loaded into a transport over-pack. Steady state thermal simulations are performed for a range of fuel heat generation rates, for both nitrogen and helium cover gas, and different fuel cladding emissivities. Computational fluid dynamics (CFD) simulations are employed to calculate buoyancy induced fluid motion in, and natural convection and radiation heat transfer across, all gas filled regions. The results are compared to stagnant-gas CFD (S-CFD) simulations, and to simulations that employ Effective Thermal Conductivities (ETC) in the fuel regions. Two narrow gas-filled gaps, between the fuel basket and its support brackets, and between the MPC and the transport over-pack, account for a significant faction of the total thermal resistance between the hottest fuel and the environment. Those gap thermal resistances are strongly affected by the cover gas. The cask Thermal Dissipation Capacity (TDC) is defined as the fuel heat generation rate that causes the fuel cladding to reach its allowed temperature limit. The TDC predicted by stagnant-gas calculations is essentially the same as that predicted by the CFD simulation, and 6% higher than that predicted by the ETC model. The TDC is 27% larger when helium is the backfill gas than when nitrogen is used. A ten percent increase in cladding emissivity leads to less than a 1% increase in the TDC. The non-isothermal surface temperature profiles of the basket openings determined in this work will be used in future simulations and benchmark experiments.

## INTRODUCTION

The goal of this work is to develop improved analytical tools to predict the temperature of spent nuclear fuel cladding inside transport casks. Spent nuclear fuel is transported away from reactor sites in gas-filled casks that are designed to provide protection during normal and accident conditions [1, 2]. Modern truck or rail casks transport up to 4 or 21 Pressurized Water Reactor (PWR) assemblies, respectively. The fuel assemblies consist primarily of long zircaloy rods held in a square array by periodic spacer plates [3]. The majority of rods contain $UO_2$ fuel pellets. These pellets remain highly radioactive and generate heat after the assembly is removed from a reactor. The rates of radioactive decay and heat generation decrease with time after removal.

During transport the zircaloy cladding that surrounds the fuel pellets must not exceed 400ºC to avoid the possible formation of radial hydrides which may compromise containment integrity [4]. The peak cladding temperature (PCT) for a given payload must be accurately predicted to assure this temperature is not exceeded. This limitation requires the fuel heat generation Q be below a certain level. In the current work, we define the cask Thermal Dissipation Capacity (TDC) as the total fuel heat generation rate that brings the fuel cladding to its temperature limit.

Finite element thermal analysis is generally used to predict PCT for a given payload [1, 2, 5]. In the past, computational resources were not readily available to accurately model the many fuel rods within a cask. A number of Effective Thermal Conductivities (ETC) were developed to model conduction and radiation heat transfer within the fuel regions of the cask in the direction normal to the fuel rod axes [1, 6, 7, 8]. These models neglect natural convection and a number of other effects. Finite element cask models that use these models overestimate the cladding temperature and so underestimate the cask TDC. This can cause operators to age spent fuel for longer time periods than are actually required, and/or put fewer assemblies in a cask than can be safely transported. Under-loading casks increases the number of shipments, the risk of accidents, and costs.

Modern computational resources allow two-dimensional cask models to accurately represent the fuel rods. Venigalla and Greiner [9] performed two-dimensional thermal simulations of a truck cask designed to transport four PWR assemblies. The model included 15x15 arrays of fuel rods within the square cross section openings that support the fuel. Computational fluid dynamics (CFD) simulations calculated buoyancy induced motion within, and natural convection and radiation heat transfer across, the gas filled regions. Stagnant-gas CFD (S-CFD) simulations, with zero gas speed, were compared to the CFD results to evaluate the effect of gas motion. Simulations using ETCs in the fuel region were performed for comparison. The cask Thermal Dissipation Capacity (TDC) was predicted for helium (He) and nitrogen ($N_2$) cover gas using all three fuel region models. The cask TDC is 23% higher for helium than for nitrogen. The TDC from the CFD and S-CFD models were nearly identical, which indicates that gas motion does not significantly affect heat transfer. The TDC from the ETC model was 6% lower than that predicted by CFD. Increasing the cladding emissivity by 10% increases the TDC by 4% for nitrogen, but only 2% for helium. The basket surface temperatures calculated in that work were highly non-isothermal. They can be used as boundary condition in future benchmark experiments.

The US Department of Energy has proposed using a Transport, Aging and Disposal (TAD) canister system for future transport campaigns [10]. In that system, fuel is loaded into a canister which is then filled with a non-oxidizing cover gas and sealed at a reactor side. The canister is then loaded into a transport over-pack. That system has similarities to the Multi-Purpose Canister (MPC) conceptual design [2].

In the current work, a two-dimensional finite volume model of a multi-purpose canister, designed to hold 21 PWR assemblies, within a rail over-pack is constructed [2]. Steady state thermal simulations are performed for a range of fuel heat generation rates, for both nitrogen and helium cover gas, and different fuel cladding emissivities. CFD simulations are employed to calculate buoyancy induced fluid motion in, and natural convection and radiation heat transfer across, all gas filled regions. The results are compared to stagnant-gas simulations, and to simulations that employ effective thermal conductivities (ETC) in the fuel regions. Details of this work are found in the thesis by Gudipati [11]

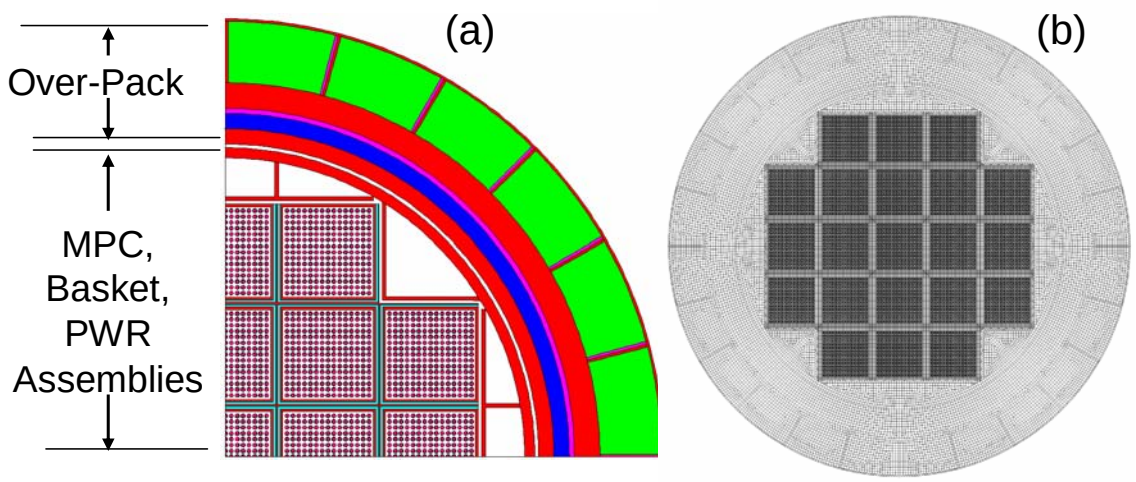


**Figure 1. (a) One-quarter cross section of a 21-PWR MPC Rail Cask. (b) Full cross section finite volume model used in current simulations.**

## COMPUTATIONAL MODEL

Figure 1a shows one quarter of the cross section through a 21-PWR MPC rail cask [2]. It represents a plane halfway between the cask ends. The dot-filled regions represent 15x15 PWR fuel assemblies inside the basket openings. All 225 fuel rods in each assembly are identical. Each is a zircaloy cladding tube of outer diameter 10.7 mm and wall thickness 0.67 mm, containing $UO_2$ pellets. No gap is modeled between the pellets and cladding. The center-to-center pitch of the rods is 14.4 mm. The fuel assemblies are similar to a Babcock & Wilcox 15x15 Mark B PWR [3] but do not contain unheated components.

The fuel assemblies are supported in a basket. The basket is a grid of square cross section tubes. The interior openings, where fuel is placed, are 22.35 cm wide and tall. The fuel assemblies are assumed to be "floating" in the openings so that the distance between the center of the outermost rods and the basket wall is 9.82 mm. The inner surface of each basket tube is 0.6-cm-thick stainless steel. It is surrounded by 0.6-cm-thick borated aluminum, which is surrounded by 0.2-cm-thick stainless steel. Several L-shaped and T-shaped brackets are between the basket outer surface and the MPC. There are 0.6-cm gaps between the basket and the brackets, and 8.48-mm-thick gaps between the brackets and the MPC.

The MPC is 2.54-cm-thick stainless steel and has a 148-cm inner diameter. It is separated from the 3.8-cm-thick stainless steel cask inner liner by a 0.8-cm-thick gap. The liner is surrounded by a 3.8-cm-thick layer of depleted uranium and a 1.27-cm-thick layer of lead, which are gamma-shielding materials. These components are surrounded by a 6.36-cm-thick stainless steel cask body. A 15.24-cm-thick polypropylene neutron shield, which is covered by a 0.63-cm-thick stainless steel skin, encircles the package. Stainless steel and copper radial fins, both of thickness 0.6 cm, support the outer skin.

Atmospheric pressure cover gas fills the open spaces within the cask. There are three open spaces: (1) within the basket openings; (2) between the basket outer surface and MPC inner surface; and (3) between the MPC outer surface and transport cask inner surface. In the current work different simulations are performed for helium or nitrogen cover gases in these spaces. Temperature-dependent thermal conductivities are applied to all solid and gas components [1, 2]. The basket wall emissivity is $\varepsilon_w = 0.57$. Several different cladding emissivities are presented in the literature [6, 8]. The cladding emissivity used in the majority of the current simulations is $\varepsilon_c = 0.8$. Simulations were performed for the range $\varepsilon_c = 0.7$ to 0.9 to determine its effect on the results.

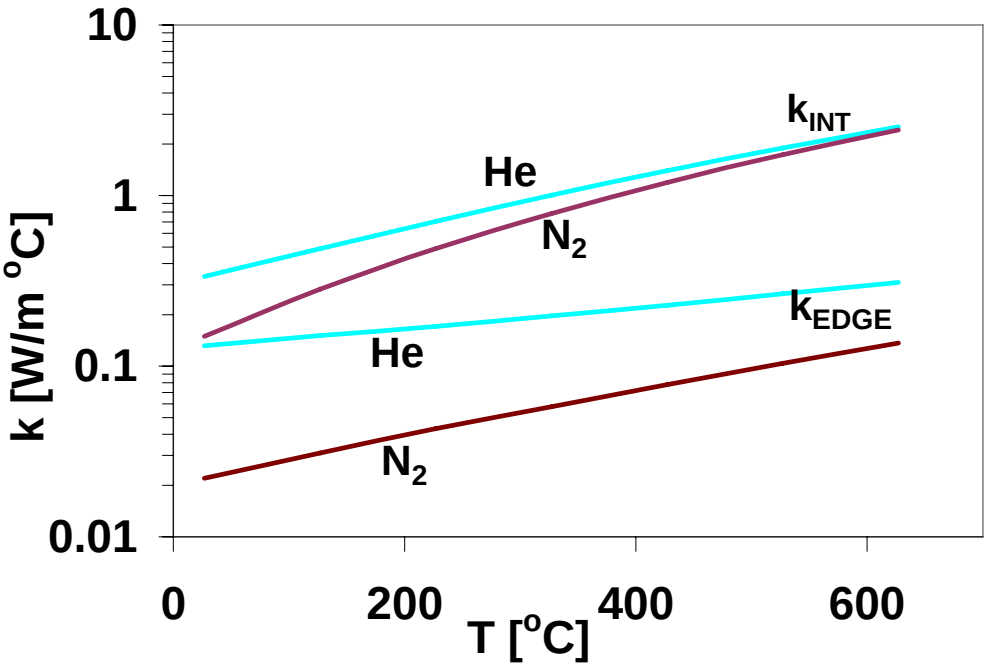


**Figure 2. Interior and edge region effective thermal conductivities (ETC) for a 15x15 PWR in He and $N_2$ cover gases [7].**

Figure 1b shows a two-dimensional finite volume grid used to simulate the entire cask cross section. It was constructed using the Patran finite element package. Nominal and fine grids, with 159,720 and 647,484 elements respectively, were used to evaluate mesh independence. All simulations are performed by importing these meshes into the Fluent computation package. Fluent utilizes the finite volume method to solve the governing mass, momentum and energy equations. A second-order upwind discretization scheme is used to solve the momentum and energy equations along with SIMPLEC algorithm for pressure velocity coupling.

The current simulations use three different fuel region models. The first are CFD simulations that include buoyancy-induced motion in all the gas filled gaps. The second are Stagnant-gas CFD (S-CFD) simulations that assume the gas speed is zero. Both these models include the effects of radiation heat transfer across all gaps. The third are Effective Thermal Conductivity (ETC) simulations that employ conductivities developed by Manteufel and Todreas [7] inside the basket openings, and radiation and stagnant-gas conduction across the other gas fill regions. In that model each basket opening is divided into a 21.7-cm by 21.7-cm interior square that represents the fuel, and an outer edge of thickness 0.3 cm that represents the gap between the fuel and basket. The temperature-dependent conductivities applied to these interior and edge regions $k_{INT}$ and $k_{EDGE}$ are given for helium and nitrogen cover gases in Fig. 2. They are applied to the appropriate elements in Fig. 1b.

For the CFD and S-CFD calculations, a uniform volumetric heat generation is applied to all the fuel pellets. It is determined by dividing the *total* heat generation rate of fuel within the cask Q by the number of assemblies (21) and the total volume of each assembly's fuel pellets (0.05 $m^3$, based on a rod length of 3.601 m), multiplied by a peaking factor of 1.25 [3]. The peaking factor accounts for the higher heat generation in the midsection of the PWR assembly compared to its average. For the ETC simulations, the volumetric heat generation rate is applied

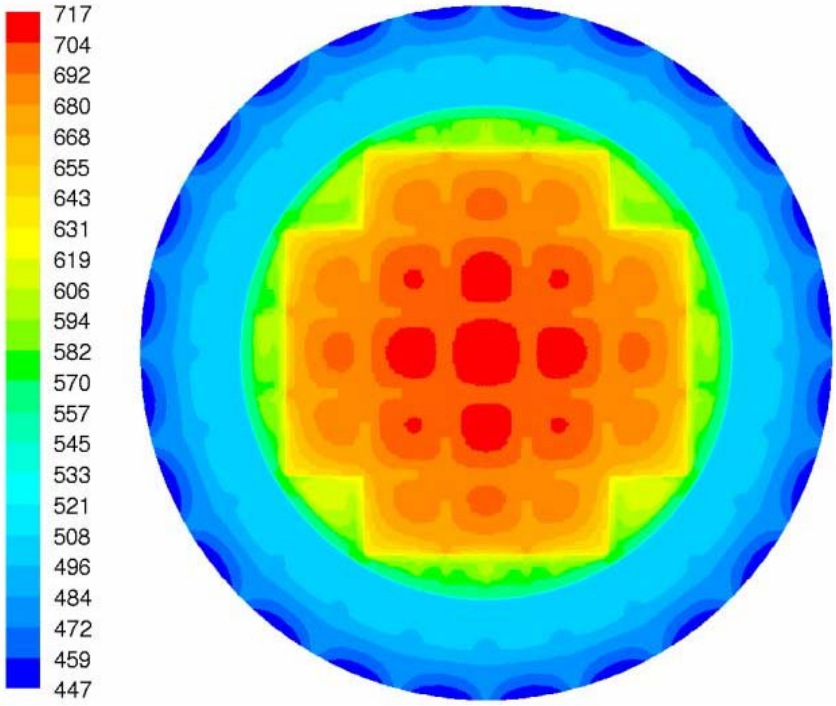


**Figure 3. Temperature contours (in Kelvin) for Q = 17.6 kW for $N_2$ cover gas from a CFD simulation**

to the interior square region. It is determined using the effective fuel volume (the area of the interior square region times the rod length).

For all simulations, the cask exterior surfaces are exposed to normal hot day conditions consisting of still air at 38°C with a constant solar heat flux of 388 W/m$^2$ on the entire surface [12]. This work does not employ reduction in flux based on diurnal variations, regions facing toward or away from the sun, or solar absorptivity (these factors may be included in future work). The package radiates to the environment with a surface emissivity of 0.2 [2]. Natural convection heat flux from the surface is calculated using a Nusselt number correlation for a horizontal cylinder [13].

## RESULTS

Figure 3 shows temperature contours for a total fuel heating rate of Q = 16.8 kW (800 W/assembly) with $N_2$ cover gas from a CFD simulation. Buoyancy-induced gas motion causes the hottest location to be slightly above the cask center. The maximum cladding temperature is 443ºC, which is above the allowed limit of 400ºC. This indicates that the cask thermal dissipation capacity $Q_{TDC}$ is less than 16.8 kW.

Figure 4 shows the temperature within the cask versus distance from the cask center along diagonal lines that are 45º above and below the horizontal (the upper diagonal is shown in the figure inside the plot). Both of these lines pass through two basket openings. They then pass through the triangular-shaped, gas-filled channels between the basket and the MPC, the MPC, the gas-filled annular gap between the MPC and over-pack, and then through the over-pack itself. Results are shown for all three fuel region models (CFD, S-CFD and ETC) and both cover gases ($N_2$ and He).

The temperatures in the over-pack (r > 0.77 m) are nearly identical for both gases and all three models. The temperature inside the over-pack inner surface is higher when $N_2$ is the cover gas than when He is used. This difference is due to $N_2$'s lower thermal conductivity. The CFD

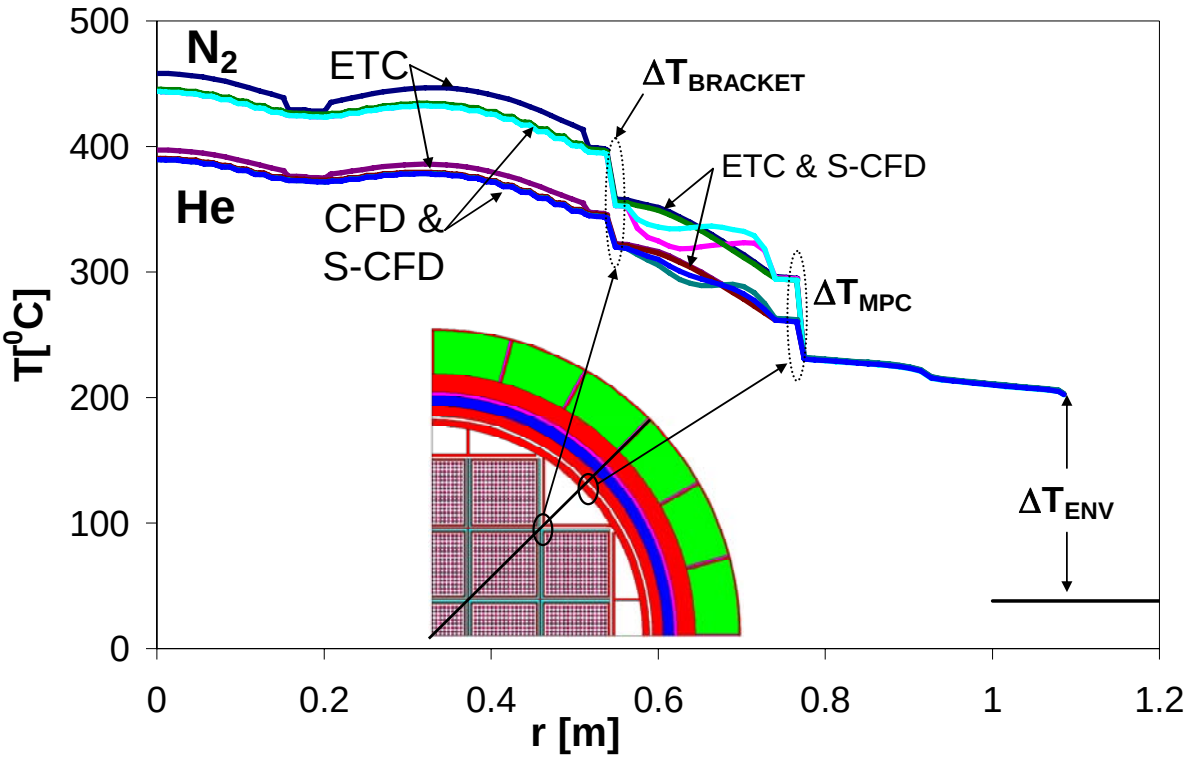


**Figure 4. Cask temperature versus distance from cask center along diagonal lines that are 45° above and below the horizontal. Results are included for He and $N_2$ cover gases as predicted by CFD, S-CFD and ETC models.**

results on the upper diagonal are slightly warmer than those on the lower because those simulations include the effects of buoyancy-induced gas motion. However, the only places where the upper and lower diagonal results are significantly different are in the gas-filled channels between the brackets and MPC. The S-CFD results from the upper and lower diagonal are identical because that model does not include gas motion. The S-CFD temperatures in the fuel are only slightly warmer than those from the S-CFD simulation. This suggests that gas motion does not strongly affect heat transfer.

The ETC simulation predicts higher temperatures in the fuel than the other models. The slope of the ETC results in the interior of the basket openings is very close to those from the CFD and S-CFD simulations. However, the ETC slope near the edge of the basket openings is steeper. This high slope appears to be caused by the low value of the effective thermal conductivity in the gap around each fuel element (see Fig. 2).

Figure 4 shows three locations in the cask where the temperature exhibits large steps. Two are in the gaps between the basket and brackets (marked $\Delta T_{BRACKET}$ in the figure) and between the MPC and Over-pack ($\Delta T_{MPC}$). These temperature differences are nearly the same at different angular positions around the cask because the components are assumed to float (there is no solid to solid contact). The thermal resistance in the gap between isothermal internal and external cylinders decreases as their surfaces approach each others. This suggests that the temperature differences between the basket and brackets, and between the MPC and over-pack, would be smaller under the more realistic condition of them nearly touching or in contact near the bottom of the cask. The third location where the temperature profile exhibits a step is

| | $\Delta T_{BASKET}$ | $\Delta T_{GAP}$ | $\Delta T_{ENV}$ | $\Delta T_{TOTAL}$ |
|---|---|---|---|---|
| $N_2$ | 41ºC | 63ºC | 164ºC | 405ºC |
| He | 23ºC | 30ºC | 164ºC | 351ºC |

**Table 1. Temperature steps for $N_2$ and He with Q = 16.8 kW from a CFD simulation**

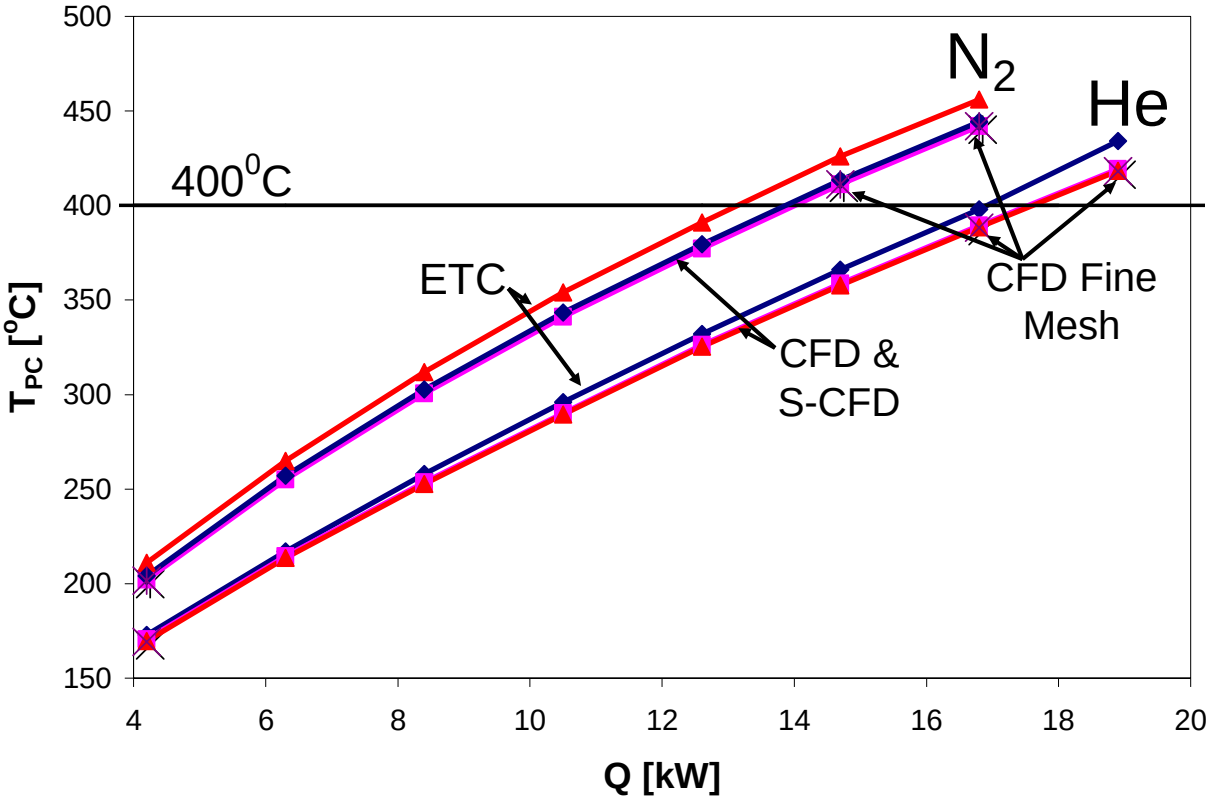


**Figure 5. Peak cladding temperature versus heat generation rate predicted by CFD, S-CFD and ETC models for He and $N_2$ cover gases.**

between the cask's outer surface and the environment ($\Delta T_{ENV}$). In the current work, the maximum possible solar heat flux is absorbed by the cask. This temperature difference would be smaller if a smaller solar heat flux was absorbed.

Table 1 summarizes the values of $\Delta T_{BRACKET}$, $\Delta T_{MPC}$, $\Delta T_{ENV}$, and $\Delta T_{TOTAL}$ for He and $N_2$ gases from the CFD simulation with Q = 16.8 kW. The total temperature difference $\Delta T_{TOTAL}$ is the difference between the hottest fuel and the environment. The sum $\Delta T_{BRACKET}$ + $\Delta T_{MPC}$ + $\Delta T_{ENV}$ is greater than 60% of $\Delta T_{TOTAL}$. This indicates that uncertainty in $\Delta T_{BRACKET}$, $\Delta T_{MPC}$, and $\Delta T_{ENV}$ can significantly affect the predicted peak cladding temperature (PCT). The effect of assuming near contact between interior components on $\Delta T_{BRACKET}$ and $\Delta T_{MPC}$, and different solar heat flux absorption assumptions on $\Delta T_{ENV}$ may be considered in future work.

Figure 5 shows the peak cladding temperature (PCT) versus fuel heat generation rate. Predictions from all three models (CFD, S-CFD and ETC) and for both cover gases ($N_2$ and He) are included from simulations using the nominal mesh. Fine mesh CFD results are also included. The agreement between the fine and nominal mesh results indicates the CFD simulations are mesh-independent.

| | $Q_{TDC}$ [kW] | |
|---|---|---|
| | CFD & S-CFD | ETC |
| Nitrogen | 13.9 | 13.1 |
| Helium | 17.6 | 17.0 |

**Table 2. Cask thermal dissipation capacities determined from CFD, S-CFD and ETC models for nitrogen and helium cover gases**

For a given fuel heat generation rate the peak cladding temperature is lower when helium is the cover gas than for nitrogen. This is caused by helium's higher thermal conductivity. For both nitrogen and helium, the CFD and S-CFD results are nearly identical. This indicates that buoyancy induced gas motion does not strongly affect heat transfer for the full range of Q investigated in this work. The CFD and S-CFD peak cladding temperatures are somewhat lower than those predicted from the ETC model. As noted earlier, however, uncertainties in the assumptions regarding contact between solid components and absorption of solar heat flux may affect these results significantly.

The horizontal line at 400ºC shows the cladding temperature limit [4]. The cask thermal dissipation capacity ($Q_{TDC}$) is determined from the point where the peak cladding temperature crosses this line. Table 2 summarizes the cask thermal dissipation capacity for helium and nitrogen from all three models. The CFD and S-CFD models indicate $Q_{TDC}$ is 27% higher when helium is the cover gas as compared to nitrogen. Moreover, the CFD and S-CFD models predict $Q_{TDC}$ values that are 4% to 6% higher than those from the ETC models.

Basket Surface Temperature Profiles

Benchmark experiments are required to evaluate the accuracy of CFD simulations for predicting radiation/natural convection heat transfer in basket openings and clad temperatures. These experiments must be performed in enclosures whose temperatures are close to the basket temperatures that exist in casks. The basket temperatures determined in the current simulations are presented in this section and may be used to design future benchmark experiments.

Figure 6 shows the five basket openings along the vertical centerline of the cask, and the eight openings on its right side. Based on symmetry, the results from the eight openings on the left side are a mirror image of the ones to the right, and so they are not shown in the figure. The thirteen basket openings in Fig. 6 are labeled A though M.

Figure 7 shows the basket surface temperature versus cord-coordinate S from the CFD simulations. Results for nitrogen and helium are presented in Figs. 7a and 7b, respectively. For each gas the fuel heat generation rate is the cask thermal capacity for that gas, as given in Table 2. The S-coordinate for each basket opening is the distance along cords on its surface. For each basket S = 0 is the surface location closest to the cask center. Opening C is divided into eight segments. For each, S = 0 is at the middle of each wall and S = 11.175 cm is at each corner. All other openings are subdivided into two segments. For openings A, B, D, E, H and L, location S = 0 is at the middle of the wall closes to the cask center and S = 44.7 cm is at the middle of the opposite wall. For openings F, G, I, J, K and M, location S = 0 is at the corner closest to the cask center and S = 44.7 cm is at the farthest corner.

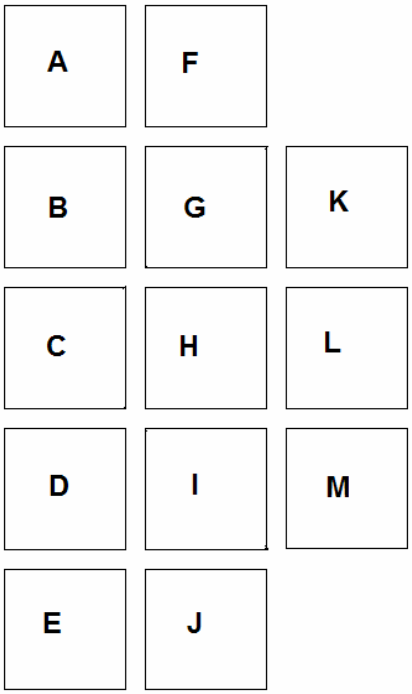


**Figure 6. The Fuel Baskets openings along the vertical centerline and right side of the cask are labeled A to M for identification purposes.**

The results for all eight cords in basket opening C are presented in Fig. 7a for nitrogen and Fig. 7b for helium. On the scale of Figure 7 the results from all eight cords are identical. Examination of the data shows that buoyancy-induced gas motion causes the upper cords to be slightly warmer than the lower ones. The results from openings B, D and H (two cords each) also group together. Gas motion actually causes opening B (in the upper portion of the cask) to be slightly warmer than the lower ones. Similarly, the results from openings G and I are a group, as are the results from openings A, E, and L, and openings F, K, J, and M. The last set of openings is not bisected by horizontal, vertical, or diagonal lines passing through the cask center. As a result, the temperature profiles along different cords within those openings are not close to each other.

Figure 7 shows that basket openings closer to the cask center have higher average temperatures, and are more isothermal than openings closer to the package outer surface. The average surface temperature ranges from 381°C at the center of the cask to 347°C near its periphery. The surface temperature's non-uniformity (difference between the maximum and minimum) ranged from 1°C in the center to 43°C at the periphery. These temperatures will be used in future benchmark experiments.

Dependence on Clad Emissivity

The simulations presented in this work were repeated with a range of cladding emissivities. For a given fuel heat generation rate, increasing the emissivity decreases the peak cladding temperature. As a result, increasing the clad emissivity increases the cask thermal dissipation capacity. Figure 8 shows the ratio of cask thermal dissipation capacity for a given fuel cladding emissivity to the value for cladding emissivity equal the baseline value (0.8) versus cladding emissivity. Results are from the CFD calculations for He and $N_2$ cover gases. The results show that a 10% increase in the cladding emissivity results in less than a 1% increase in TDC. These results may be affected significantly if different assumptions are made about internal component contact, and/or solar heat flux absorption.

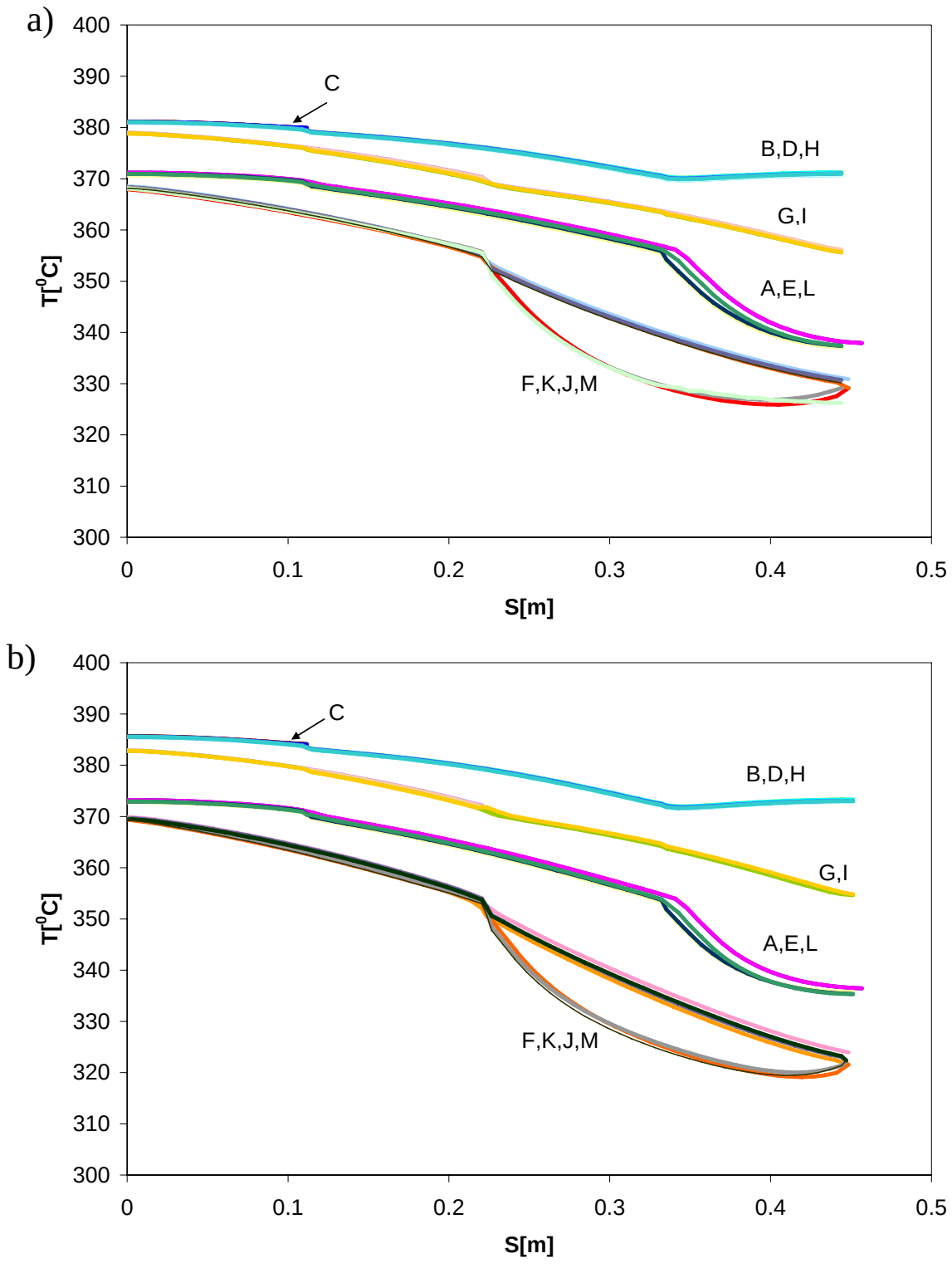


**Figure 7. Basket opening surface temperature profiles versus surface coordinates a) Nitrogen at Q = 13.9 kW (662 watts/assembly) and (b) Helium at Q = 17.6 kW (840 W/Assembly)**

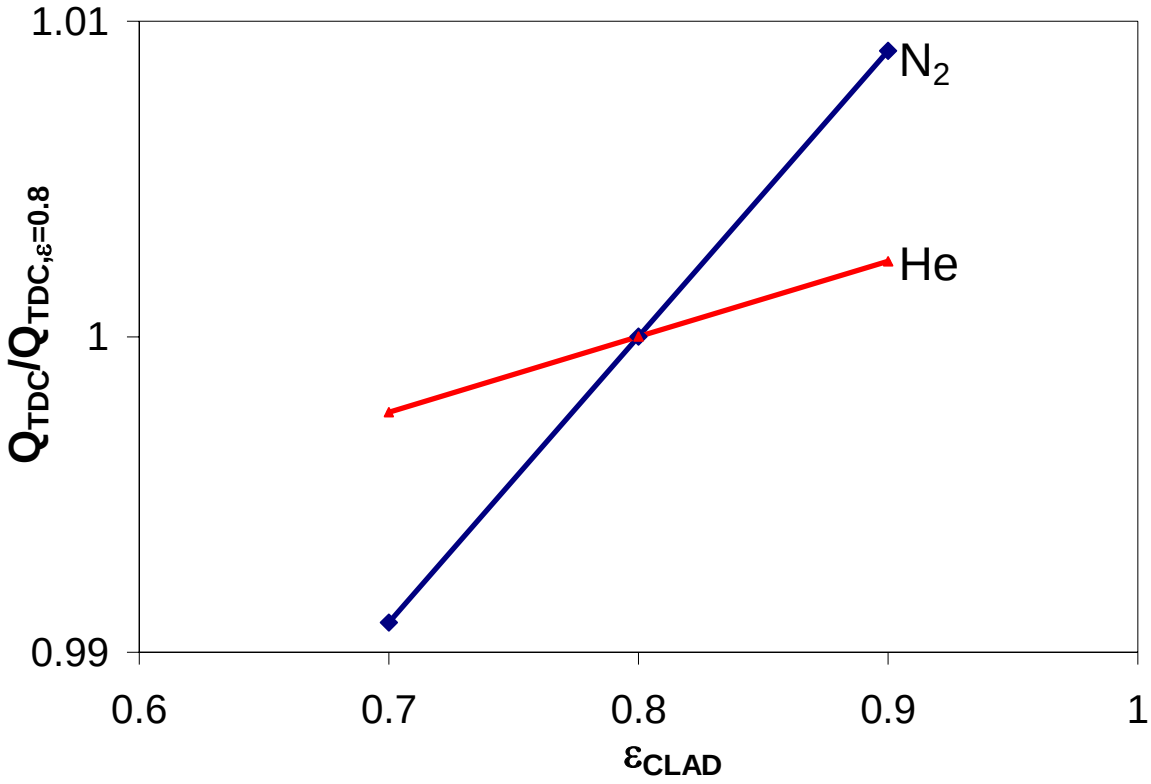


**Figure 8. Ratio of cask thermal dissipation capacity for a given fuel cladding emissivity to the value for cladding emissivity equal the baseline value (0.8) versus cladding emissivity . Results are from the CFD calculations for He and $N_2$ cover gases.**

## CONCLUSIONS

A two-dimensional, finite volume model of a 21 PWR Multi-Purpose Canister (MPC) inside a rail cask was constructed. In that cask, fuel is loaded into a basket structure inside an MPC. The MPC is sealed, filled with a non-oxidizing cover gas, and loaded into a transport over-pack. Steady state thermal simulations are performed for a range of fuel heat generation rates, for both nitrogen and helium cover gas, and different fuel cladding emissivities. Computational fluid dynamics (CFD) simulations are employed to calculate buoyancy-induced fluid motion in, and natural convection and radiation heat transfer across, all gas filled regions. The results are compared to stagnant-gas CFD (S-CFD) simulations, and to simulations that employ Effective Thermal Conductivities (ETC) in the fuel regions. Two narrow gas-filled gaps, between the fuel basket and it support brackets, and between the MPC and transport over-pack, account for a significant faction of the total thermal resistance between the hottest fuel and the environment. Those gap thermal resistances are strongly affected by the cover gas. The cask thermal dissipation capacity (TDC) is defined as the fuel heat generation rate that causes the fuel cladding to reach its allowed temperature limit. The TDC predicted by stagnant-gas calculations is essentially the same as that predicted by the CFD simulation, and both are 6% higher than that predicted by the ETC model. The TDC is 27% larger when helium is the backfill gas than when nitrogen is used. A 10% increase in cladding emissivity leads to less than a 1% increase in the TDC. The non-isothermal surface temperature profiles of the basket openings determined in this work will be used in future simulations and benchmark experiments.

## NOMINCLATURE

| | |
|---|---|
| k | Thermal conductivity |
| r | Distance from cask center |
| S | Cord-coordinate on basket surface |
| T | Temperature |
| $\varepsilon_C$ | Cladding emissivity |
| | |
| CFD | Computational Fluid Dynamics |
| ETC | Effective Thermal Conductivity |
| He | Helium cover gas |
| MPC | Multi-Purpose Canister |
| $N_2$ | Nitrogen cover gas |
| PCT | Peak cladding temperature ($T_{PC}$) |
| TDC | Cask Thermal Dissipation Capacity ($Q_{TCD}$) |
| S-CFD | Stagnant-gas Computational Fluid Dynamics |

## ACKNOWLEDGMENTS

This work was sponsored by the US Department of Energy Advanced Fuel Cycle Initiative under contract DE-FC07-06ID14782.

## REFERENCES

[1] General Atomics (GA), 1998, “GA-4 Legal Weight Truck From-Reactor Spent Fuel Shipping Cask, Safety Analysis Report for Packaging (SARP),” San Diego, California 92186-5608.

[2] Office of Civilian Radioactive Waste Management (OCRWM), US Department of Energy, 1993, “Multi-Purpose Canister (MPC) Implementation Program Conceptual Design Phase Report,” DOC ID: A20000000-00811.

[3] U.S Department of Energy, 1987, “Characteristics of Spent Nuclear Fuel, High-Level Waste, and Other Radioactive Wastes Which May Require Long-Term Isolation”, Office of Civilian Radioactive Waste Management, DOE/RW-0184.

[4] Nuclear Regulatory Commission (NRC), 2005, “Cladding Considerations for the Transportation and Storage of Spent Fuel”, Interim Staff Guidance Report for the Spent Fuel Project Office of the U.S., ISG-11 Rev. 3, available at www.nrc.gov

[5] Greiner, M., Gangadharan, K.K., and Gudipati, M. , 2006, "Use Of Fuel Assembly/Backfill Gas Effective Thermal Conductivity Models to Predict Basket and Fuel Cladding Temperatures within a Rail Package during Normal Transport," PVP2006-ICPVT-11-93742, *Proceedings of ASME Pressure Vessels and Piping Division Conference*, July 23-27, Vancouver, BC, Canada, to appear *Nuclear Technology*, 2007.

[6] Unterzuber, R., Milnes, R.D., Marinkovich, B.A. and Kubancsek, G.M., 1982, “Spent-Fuel Dry-Storage Testing at EMAD (March 1978 through March 1982),” Prepared for the US DOE Commercial Spent Fuel Management Program Office at the Pacific Northwest Laboratory, B-D3339-A-G.

[7] Manteufel, R.D., and Todreas, N.E., 1994, “Effective thermal conductivity and edge conductance model for a spent fuel assembly,” *Nuclear Technology*, Vol. 105, pp. 421-440.

[8] Bahney, R.H., and Lotz, T.L., 1996, “Spent Nuclear Fuel Effective Thermal Conductivity Report,” prepared for the U.S. DOE, Yucca Mountain Site

Characterization Project Office by TRW Environmental Safety Systems, Inc., D.I.: BBA000000-01717-5705-00010 REV 00.

[9] Venigalla, V.V.R., and Greiner, M., 2007, “CFD Simulations of Natural Convection/Radiation Heat Transfer within the Fuel Regions of a Truck Cask for Normal Transport," PVP2007-26242, *Proceedings of the 2007 ASME Pressure Vessels and Piping Division Conference*, July 22-26, San Antonio, Texas.

[10] U.S. Department of Energy Office of Civilian Radioactive Waste Management, 2007, “Transportation, Aging and Disposal Canister System Performance Specification, Revision 0,” DOC ID: WMO-TADCS-000001.

[11] Gudipati, Mithun, 2007, “Computational Fluid Dynamics Simulations of Basket and Fuel Cladding Temperatures within a Rail Cask during Normal Transport,” M.S Thesis, University of Nevada, Reno.

[12] U.S. Nuclear Regulatory Commission, 1992, “Packaging and Transportation of Radioactive Material,” Rules and Regulations, Title 10, Part 71, Code of Federal Regulations.

[13] Incropera, F.P., and DeWitt, D.P., 1996, *Introduction to Heat Transfer*, 3rd edition, J. Wiley and Sons, New York.